Journal of Building Engineering 86 (2024) 108930

Contents lists available at ScienceDirect

Journal of Building Engineering

journal homepage: www.elsevier.com/locate/jobe

Experimental and numerical investigation on the behavior of concrete sandwich slab panel for a structural system

Néstor Guerrero [a,*], Julian Carrillo [b,c], Reyes I. Herrera [d], MaríaE. Marante [d,e]

[a] *Department of Civil Engineering, Universidad de Ibagué, Ibagué, Colombia*
[b] *Department of Civil Engineering, Universidad Militar Nueva Granada, Bogotá, Colombia*
[c] *Colombian Earthquake Engineering Research Network, CEER, Bogotá, Colombia*
[d] *Structural Engineering Department, Universidad Centroccidental Lisandro Alvarado, Barquisimeto, Venezuela*
[e] *Construction and Sustainable Development Department, Universidad Metropolitana, Caracas, Venezuela*

A R T I C L E I N F O

Keywords:
Concrete sandwich panel
Slab panel
Three-point bending test
Four-point bending test
Degree of composite action
Lumped plasticity model

A B S T R A C T

This paper proposes a simplified methodology based on a concentrated plasticity model to develop numerical analysis of concrete sandwich slab panels for structural systems. Also, a proposal for the determination of experimental damage and its evolution within concrete sandwich panels is formulated. To validate the proposed methodology, an experimental study was carried out on full-scale slab panels to analyze the flexural behavior. Eight specimens were subjected to three- and four-point bending tests. A cycle loading protocol with unloading up to zero load was performed. These specimens, constructed with either one or two joined panels, were used to assess the group action. Mechanical properties for structural analysis—such as strength, stiffness, degree of composite action, and effective moment of inertia—were determined. The tested specimens exhibit significant stiffness degradation, indicating a notable evolution of damage even at small plastic displacements. The proposed methodology proves to be effective and reliable for predicting the behavior of concrete sandwich panels under bending moments. The numerical simulations performed show an adequate description of slab panel behavior until the ultimate load, regardless of its simplicity.

1. Introduction

The usage of concrete sandwich panel structural systems has increased in recent years owing to their properties, including acoustic and thermal insulation, low self-weight, speed of installation, minimized formwork usage, durability, high energy efficiency, high level of quality control and allows a wide range of architectural finishing [1,2]. Today concrete sandwich panels are widely used globally in projects ranging from commercial facilities to multi-story apartment blocks [1]. The panels conforming these structural systems are mainly divided into slab and wall panels, and they consist of a core of expanded polystyrene (EPS) insulator sandwiched by two concrete wythes. The thickness of each concrete wythe depends on its structural function, concrete cover, anchorage of connectors, stripping, and finishing. The concrete wythes can be divided into structural and non-structural wythes. The structural wythe contributes significantly to the load resistance of the panel. The reinforcement of structural wythes depends on the dimensions, structural requirements, and serviceability of the panel [2]. The contribution of non-structural wythe, also called cladding or floating wythe, to the structural strength of the panel is insignificant. It is used primarily for aesthetics, weathering and to encase the insulation material.

* Corresponding author.
E-mail address: nestor.guerrero@unibague.edu.co (N. Guerrero).

https://doi.org/10.1016/j.jobe.2024.108930
Received 8 June 2023; Received in revised form 7 February 2024; Accepted 24 February 2024
Available online 26 February 2024
2352-7102/

The thickness of the non-structural wythe needs to be minimized to reduce the difference in temperature across its thickness, as well as the panel weight [2].

Several techniques have been proposed to connect wythes and keep integrated the insulation material. Such techniques include the use of welded diagonal truss wires [3–5], orthogonal steel wires [6,7], glass fiber-reinforced polymer (GFRP) shear grid or connectors [8–12], and fiber-reinforced polymer (FRP) [13–15]. The arrangement and spacing of shear connectors depend on several factors, such as desired composite action, applied load, span of the panel, and type of shear connectors used. Connectors can be divided into two major categories: shear and non-shear connectors. Shear connectors are those that can transfer longitudinal shear force, which results from the flexure in the panel, from one wythe to another. These connectors may resist shear in one or two perpendicular directions. On the other hand, non-shear connectors can transfer only a negligible fraction of longitudinal shear from one wythe to another [2].

The structural behavior of panels depends on the strength and stiffness of the connectors. The panels can be categorized into fully composite, partially composite, and non-composite panels, according to the degree of composite action achieved in the system [2,3]. Fully composite panels are those panels whose wythes are connected in such a way that both wythes resist the applied flexural loads and performs as an integral section, which is achieved by providing enough shear connectors between the two wythes. The failure mode of a fully composite panel is controlled either by concrete crushing or steel reinforcement yielding without failure of the connectors. In partially composite panels, the shear connectors transfer only a fraction of the longitudinal shear required for fully composite panels. In this case, the failure of the connectors is observed before concrete crushing or yielding of the reinforcement. In non-composite panels, the two concrete wythes are joined by connectors that cannot transfer the longitudinal shear force. If the two concrete wythes have the same stiffness and reinforcement, each of them would resist 50% of the total load. However, in most non-composite panel systems, the applied loads are resisted by only one of the two wythes [2,3].

Different experimental programs have been developed to identify the mechanical properties of panels such as failure modes and behavior of different types of concrete sandwich slab panels. The most widely used method of determining the flexural moment capacity is the four-point bending test (4PBT) [1,3,4,6,8–10,12–14,16]. However, other studies have performed the three-point bending test (3PBT) to assess the shear force capacity of the panel [5,15]. Both methods have been used to evaluate the strength of shear connectors between the external concrete elements of the panels [3,4,12,13,15]. Acharya et al. [17] conducted experimental testing of full-scale slab panels with three different span lengths (short, medium, and long) using 4PBT to investigate flexural behavior, strength, ductility, and failure mechanisms. Testing showed good performance of panels under gravity loads; however, the total moment capacities for the unmodified medium- and long-span specimens were significantly reduced when compared with the capacity of the short-span specimens. The short-span specimens satisfied some of the building code criteria for residential concrete floor and roof slabs without additional flexural reinforcement.

The determination of the Degree of Composite Action (DCA) in structural panels is crucial and is commonly assessed through flexural tests, considering both stiffness and strength parameters. Pessiki and Mlynarczyk [18] introduced a methodology to quantify composite action by analyzing deflection measurements during the panel's linear elastic behavior. This involves deriving the experimental moment of inertia (I_{exp}) and contrasting it with the theoretical fully composite (I_c) and non-composite (I_{nc}) moments of inertia. Zheng et al. [19] have highlighted certain considerations affecting DCA determination based on stiffness, such as loading symmetry and concrete strength, restricting its applicability to the elastic phase of Precast Concrete Sandwich Panels (PCSP). Alternatively, the strength-based calculation of DCA, pioneered by Benayoune et al. [3], postulates the strength capacity of a non-composite section as the sum of the resistance capacities of individual concrete wythes. In cases of fully composite action, both concrete wythes are treated as a singular entity, similar to a solid slab featuring dual layers of reinforcement. This approach allows for determining DCA across both elastic and ultimate phases of the panel's behavior. Choi et al. [8] and Tomlinson with Fam [20] have observed significant disparities when comparing the DCA obtained from strength-based methods versus the stiffness-based approach advocated by Pessiki and Mlynarczyk [18] for identical panels. Additionally, Zheng et al. [19] stress that the stiffness-based method is more suitable for calculating PCSP with lower DCAs, while the strength-based method is better suited for PCSP with higher degrees of composite action.

The literature on numerical simulations of concrete sandwich panels shows a wide implementation of continuum FE model. Concrete sandwich panels have been modeled for different purposes including non-linear 3D FE models with 3D deformable solids [3,10,12,13,21]. It has been also implemented in 3D FE models with shell elements to simulate concrete wythe behavior [5,9,22–24]. More simplified models that include the use of beam in the model have been also implemented to understand the mechanical behavior of this type of structural element [6,20,25,26]. Bai and Davidson [28] proposed a rigorous discrete analysis model for composite structures. The continuum FE model is the most sophisticated and provides the most detailed global and local response but requires more time and memory than other ones. The lumped plasticity model assumes that inelastic effects can be concentrated in special locations called plastic hinge; this model provides the simplest and computationally efficient approach for the nonlinear analysis of structures. Nevertheless, this approach needs calibration with experimental data.

Cipollina and Flórez-López. [27], initially oriented to the development of behavior models of reinforced concrete structures, proposed a simple experimental procedure. This procedure aims to identify yield and damage functions required for the formulation of simplified models based on lumped damage mechanics. This study adapted the variation of the modulus of elasticity method from continuum damage mechanics theory to lumped damage mechanics for assessing flexural damage, where the experimental measurement of a member stiffness is defined as the slope of unloading line in the load-displacement curve.

The lack of information such as strength capacity, stiffness and other properties required to analyze constructed buildings with this type of structural system has created challenges. Factors such as the high cost associated with full-scale testing, the difficulties of creating small-scale models, and the reluctance of many producers to share product information contribute to this knowledge gap [2,3]. This gap has been highlighted by some authors [4,6] who emphasize the importance of conducting both experimental and numerical studies. These efforts are aimed at developing reliable design guidelines for practical applications of insulated concrete sandwich panels.

Due to the necessity of implementing simplified and computationally efficient numerical models to analyze and evaluate the structural behavior of buildings constructed with slab concrete sandwich panels, this study proposes a simplified methodology based on concentrated plasticity to develop numerical analysis of this structural system. In order to validate the proposed methodology, an experimental study was carried out on full-scale slab panels to analyze the flexural behavior. Eight specimens subjected to transversal loading were tested according to established standard procedures. These specimens were constructed with either one or two joined panels and are used to assess group action. Essential properties for structural analysis—such as strength, stiffness, degree of composite action, and effective moment of inertia—are determined. In addition, a proposal for the determination of experimental damage and its evolution within concrete sandwich panels is presented.

2. Experimental program

The flexural performance of the slab panels was assessed by three- and four-point bending tests (3PBT and 4PBT). The experimental program was carried out at the Laboratory of Structural Mechanics (LME) in the Universidad Centroccidental Lisandro Alvarado (Barquisimeto-Venezuela).

2.1. Panels description

The slab panels studied in this paper are conformed to a core of expanded polystyrene (EPS) insulator sandwiched by two concrete wythes. Fig. 1 shows a view of slab panel with EPS core before cast-in-place concrete. Fig. 2 presents the geometrical characteristics of the two types of tested specimens. The total width and thickness of the slab panel is 600 mm and 235 mm, respectively, including the top and bottom concrete wythes. The Slab panels were built using an internal three-dimensional truss of 8 mm diameter wire and lateral truss shear connectors with diagonal bars of 6 mm-diameter and 0.91 mm-thick V-shaped steel sheets as top and bottom chords. This V-sheet is embedded in the concrete wythe acting as a connector between the 6 mm-diagonal and the concrete. The trusses are connected by 6 mm diameter steel bars spaced at 300 mm.

The compressive strength of the concrete of the panel was measured using three (3) cube specimens with side of 50.8 mm. The average value of compressive strength of concrete (f_c') was 19.95 MPa, and the coefficient of variation (CV) was 4.72 %. The modulus of elasticity of concrete, E_c, can be calculated using the equation ($E_c = 4700\sqrt{f_c'}$) proposed by ACI building code [29], which results in E_c = 21 GPa. The steel wire used and the steel sheet in the panels complied with ASTM A496 and ASTM A366, with yield strengths of 515 MPa, and 275 MPa, respectively. The density of the EPS core was 20 kg/m^3.

2.2. Test set-up

The test setups for 3PBT and 4PBT according to ASTM- E72 are shown in Fig. 3a and b, respectively. A servo-controlled hydraulic actuator with a capacity of 500 kN was used to apply the desired displacement histories presented in Fig. 4. As shown in this figure, a cyclic loading protocol with unloading up to zero load was performed. The specimen's support is shown in Fig. 3c and d. The actuator was mounted on a reaction frame and was connected to the specimens through a steel device, as shown in Fig. 3e and f. All the specimens were tested up to failure. Table 1 summarizes the geometrical characteristics of each specimen. Shear force and bending moment expressed as a function of the applied load P and specimen lengths L_s are included in the table.

In this study, the yield and ultimate strengths of the panels due to shear force (V_{yp} and V_{up}) and bending moment (M_{yp} and M_{up}) are determined from the experimental load-midspan deflection curves, as shown in Fig. 5a. The stiffness of slab panels during each unloading cycle (K_i) is obtained from load-displacement curves measured as the elastic slope as proposed by Cipollina et al. [30] as shown in Fig. 5b. The plastic displacement (d_p) is obtained on the elastic unloading line as the displacement corresponding to zero force. The displacement and force values were obtained directly from the actuator's data acquisition system at the point of application of the load history.

Fig. 1. Slab panel before cast-in-place concrete.

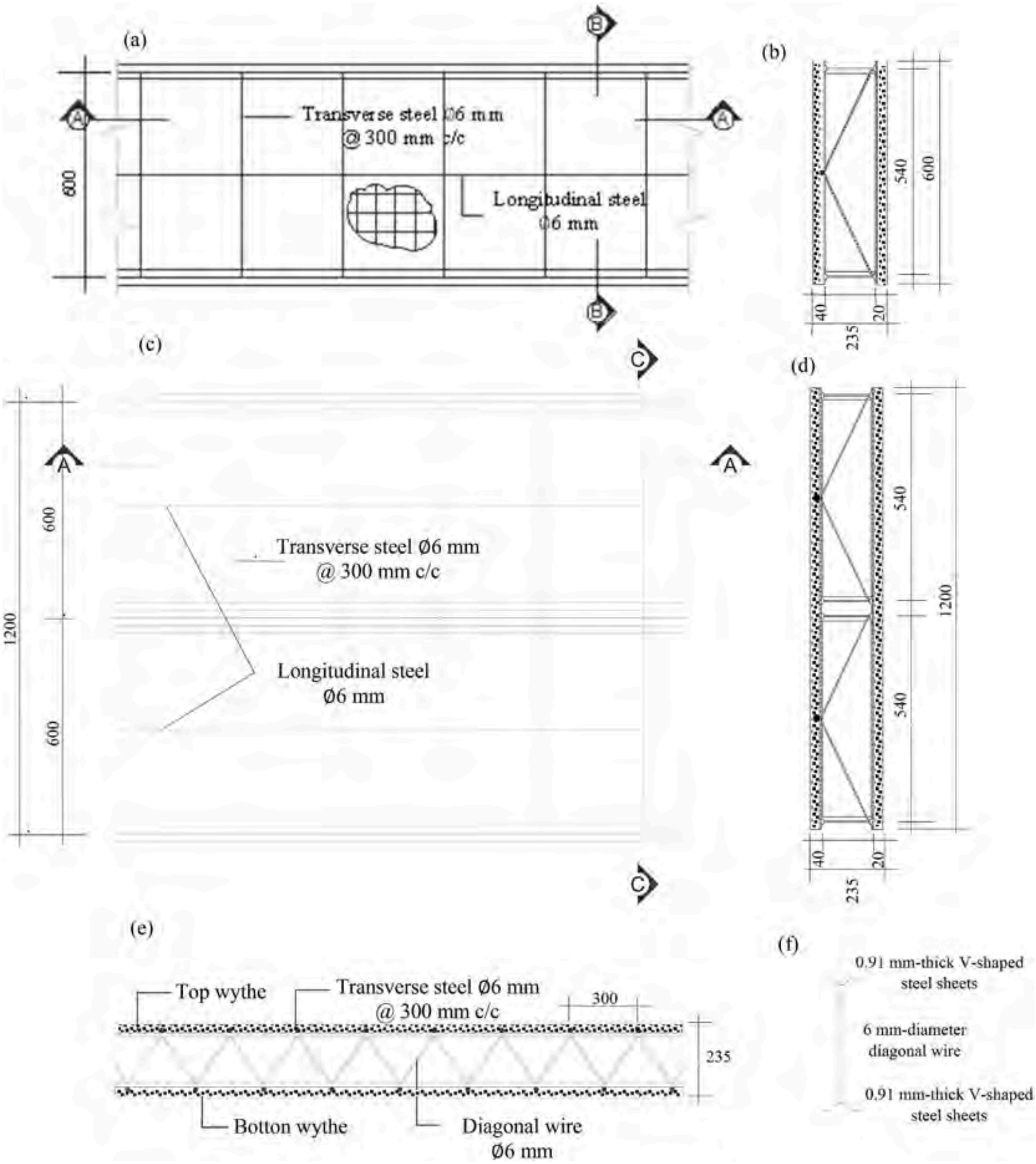

Fig. 2. Detail of tested specimens. (a) Plan view of specimen with one panel, (b) B–B transversal section of specimen with one panel, (c) plan view of specimen with two panels, (d) C–C transversal section of specimen with two panels, (e) A-A longitudinal view, (f) detail of truss shear connectors. Dimension in mm.

The flexural stiffness of a specimen in the elastic range (K_0) when subjected to the three-point and four-point bending tests is given by Eq. (1) and. (2), respectively. Then, the experimental moment of inertia (I_{exp}) for each specimen was calculated by substituting experimental values of stiffness and modulus of elasticity of concrete into Eq. (1) or (2). Furthermore, the moment of inertia (I_{expul}) before failure was determined using the stiffness value at the point of ultimate load (K_{ul}).

$$K_0 = \frac{48 E_c I_{exp}}{L_s^3} \tag{1}$$

$$K_0 = \frac{162 E_c I_{exp}}{5 L_s^3} \tag{2}$$

3. Experimental results and discussion

The test configurations allow the identification of the failure mode for each specimen. The failure criterion is determined considering the phenomenon that occurs first; the concrete crushing in the compression zone, failures on the steel elements such as

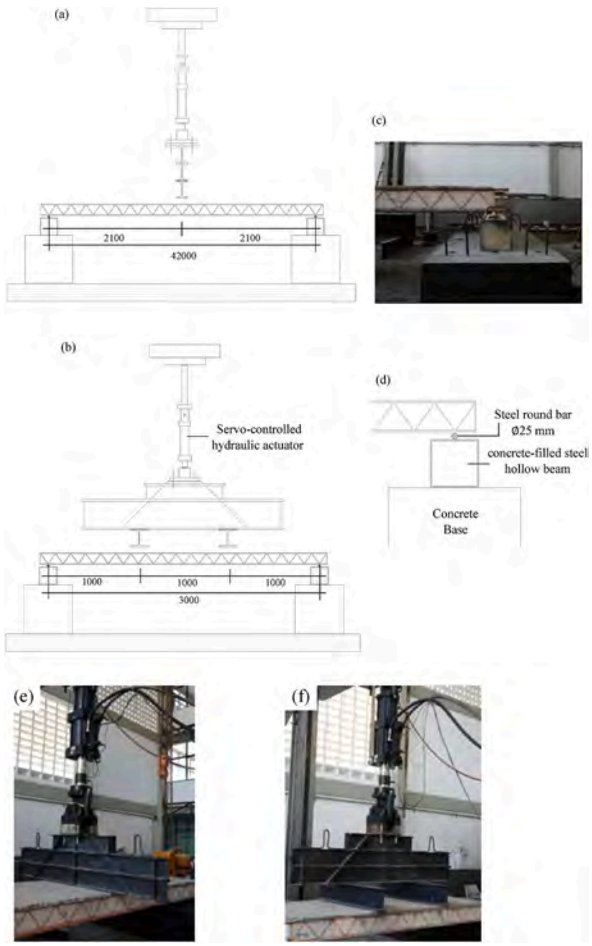

Fig. 3. Test setups: (a) elevation view of 3PBT, (b) elevation view of 4PBT, (c) specimen support, (d) 3D detail of specimen support, (e) 3D view of 3PBT, (f) 3D view of 4PBT.

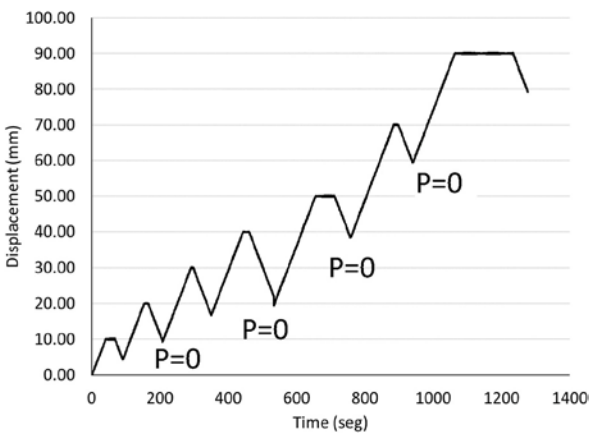

Fig. 4. Applied load history.

buckling of the diagonals of the ribs, or rupture by traction.

3.1. Three-point bending test, 3PBT

The observed failure mode in the specimens under 3PBT was characterized by tensile fracture of the V-steel sheet, which occurred

Table 1
Test matrix for bending tests (dimension in mm).

Test method	Specimen ID	Number of tests	Number of panels	Width w_s	Length L_s	Thickness			Internal Forces	
						Bottom Concrete t_b	Top Concrete t_t	Total Thickness t_s	Shear Force V	Bending Moment M
3PBT	LT2	2	1	600	4200	20	40	235	P/2	1.05 P
	LT3	2	2	1200	4200	20	40	235		
4PBT	LT1	2	1	600	3000	20	40	235	P/2	0.50 P
	LT4	2	2	1200	3000	20	40	235		

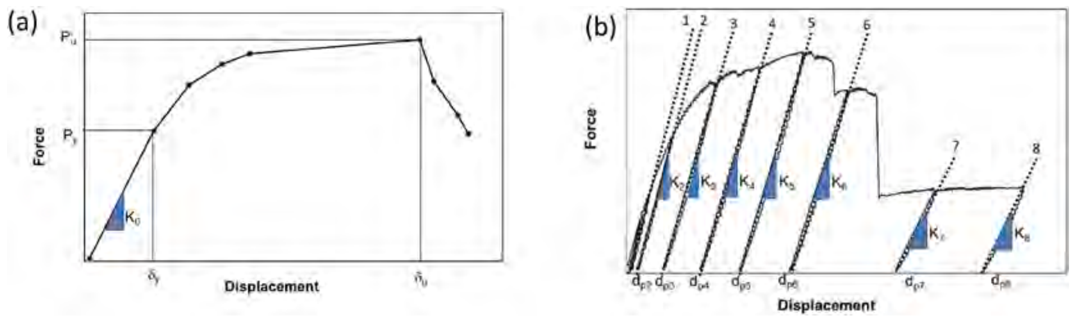

Fig. 5. Studied variables: (a) strength and midspan deflection, (b) elastic slope in unloading cycle.

at the point of the maximum bending moment after cracking of the lower wythe. The sequence of failure mode is shown in Fig. 6. Initially, bottom wythe cracking occurred as shown in Fig. 6a; after that, the crack propagated to the EPS core (Fig. 6b) and finally, the tensile fracture of the V-steel sheet took place as can be observed in Fig. 6c.

Fig. 7 shows the measured force-midspan displacement curves for specimens LT2 and LT3 and the corresponding moment-rotation curves for each specimen. The behavior observed can be divided into three stages. During the first stage, the behavior can be described as elastic up to the yield displacement (δ_y). The second stage, between the yield displacement and the ultimate displacement (δ_u), shows a defined plastic behavior due to the elongation of the V-sheet, which lasts until failure occurred with a severe decrease in strength which initiated the third stage, as shown in the sequence of images in Fig. 6. The tensile fracture of the V-steel sheet marks the beginning of this stage. Fig. 7a and b shows the graphs of the specimens with single and two slab panels, respectively. In the case of specimens LT3, the strength decrease was 37%. For specimens LT2, the decrease in strength presents significant variability in the results; 65% for specimen LT2-2 and 28% for specimen LT2-1. The envelope of load-displacement curves is shown in Fig. 7c. It is observed in this figure that the softening stage occurs at approximately 48 mm in both specimens. The corresponding envelope of moment-rotation curve is shown in Fig. 7d. As shown in the figure, the value of ultimate rotation is 0.022 rad and the yield rotation is 0.006 rad for both specimens.

Fig. 8 shows the elastic slope against plastic displacement curves; a significant stiffness degradation can be observed in each stage. The increase of stiffness in double-panel specimens can be appreciated in this figure.

The experimental results measured during 3PBT of specimens LT2 and LT3 are summarized in Table 2. The maximum midspan deflection in the single panels fulfills the standard limiting value of $l/240$ for roof members and for coupled panels fulfills the established limit ($l/360$) for members subjected to full nominal live load in ACI 318R-19 [29]. An average ductility value obtained for specimens conformed for a single panel is 3.28; the group action increased this parameter by 45%. The average ultimate load is 49% higher than the yield load in single-panel tests and 90% in double-panel tests. The stiffness values at the point of ultimate load (K_{ul}) were found to be between 10% and 22% lower than the initial stiffness values (K_0).

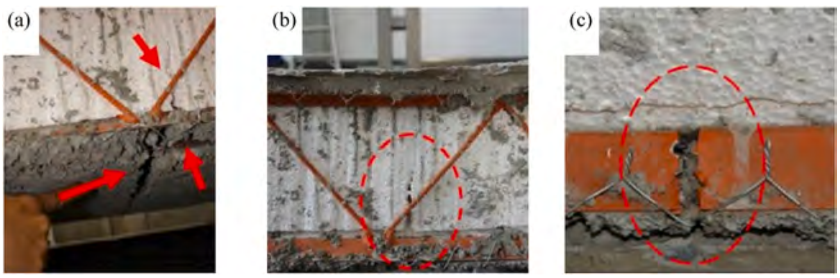

Fig. 6. Failure mode during 3PBT: (a) bottom wythe cracking fracture, (b) EPS core cracking, (c) tensile fracture of the longitudinal truss shear steel sheet.

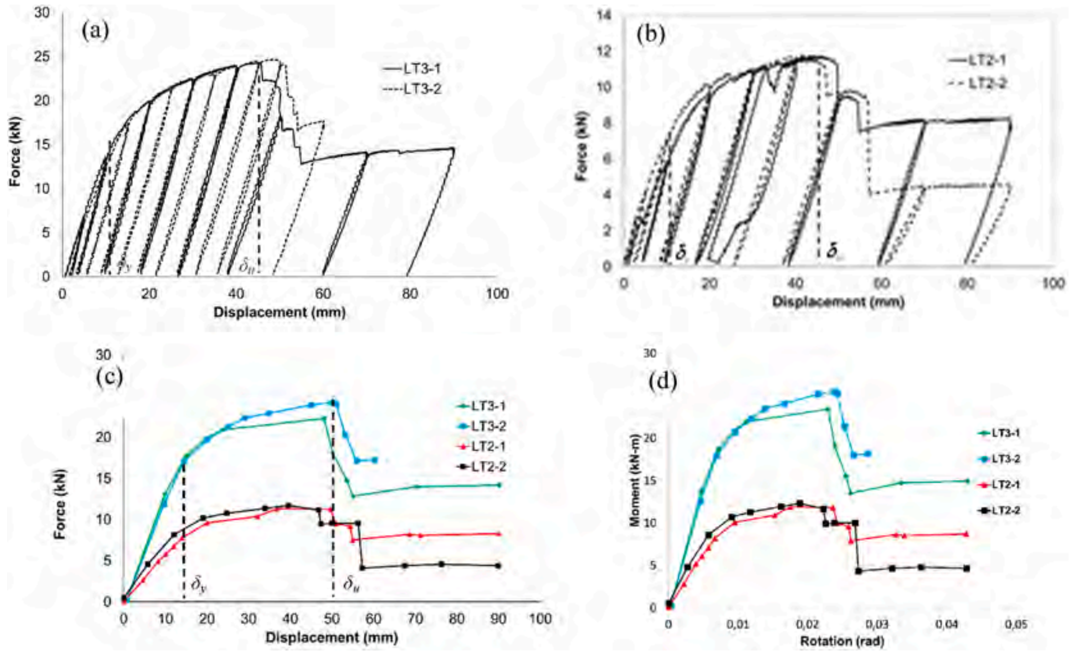

Fig. 7. (a) Force–midspan deflection of specimens LT2, (b) Force–midspan deflection of specimens LT3, (c) Force-midspan deflection envelope, (d) Moment-rotation envelope curve.

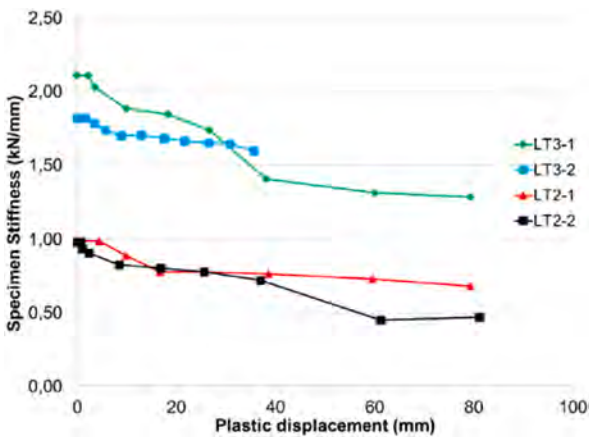

Fig. 8. Elastic slope against plastic displacement during 3BPT.

3.2. Four-point bending test, 4PBT

The observed failure mode of LT1 and LT4 specimens was buckling of the diagonals of truss shear connectors as shown in Fig. 9. This buckling is caused by the transmission of shear force to the supports and does not allow the member to develop full bearing capacity. During the test, the specimens did not show any crack in the concrete or detachment at the concrete wythes.

Fig. 10 shows the measured force-midspan deflection curves of 4PBT. It can be observed in the figure that an incipient inelastic stage was developed; however, this stage was interrupted due to the buckling of the diagonal bars. Fig. 10a and b shows the curves of single and two slab panels, respectively. In both cases, the strength decreased by approximately 25% after reaching ultimate strength. Fig. 10c shows that softening stage starts approximately at the same displacement value in all cases. The measured force–midspan deflection curves suggest a low ductility performance. Fig. 11 shows the elastic slope vs plastic displacement curves. It can be appreciated a continuous decrease of stiffness in all specimens.

Table 3 shows the results obtained from the 4PBT performed on specimens LT1 and LT4. The mean ductility obtained for a single panel is 1.42. The group action increases the ductility factor by only 12%. The mean ultimate load in specimens with two panels is 89% higher than the corresponding single panel and 83% for yielding load. The maximum deflection in all panels fulfills only the ACI 318R-19 [29] limiting value of $l/240$ for roof members.

Table 2
Parameters obtained in 3PBT.

Parameters	Unit	LT2-1	LT2-2	LT3-1	LT3-2
Yield displacement (δ_y)	mm	13.5	12.5	9.0	10.6
Span length-deflection ratio $\left(\frac{L_s}{\delta_y}\right)$		311	348	469	398
Ultimate displacement (δ_u)	mm	44.2	39.6	44.7	47.6
Ductility factor $\left(\mu = \frac{\delta_u}{\delta_y}\right)$		3.3	3.3	5.0	4.5
Yield load (P_y)	kN	7.85	7.92	12.63	13.11
Ultimate load (P_u)	kN	11.77	11.74	22.30	24.67
Ultimate-to-yield load ratio P_u/P_y		1.50	1.48	1.92	1.88
Yield shear force (V_y)	kN	3.93	3.96	6.32	6.55
Ultimate shear force (V_u)	kN	5.88	5.87	11.15	12.33
Yield bending moment (M_y)	kN • m	8.24	8.31	13.27	13.76
Ultimate bending moment (M_u)	kN • m	12.36	12.33	23.42	25.90
Elastic Flexural stiffness (K_0)	kN/mm	0.99	0.98	2.11	1.82
Experimental flexural rigidity E_cI_{exp} (10^9)	kN • mm^2	1.53	1.51	3.26	2.81
Experimental moment of inertia I_{exp} (10^6)	mm^4	72.79	72.13	155.36	133.82
Ultimate Flexural stiffness (K_{ul})	kN/mm	0.78	0.78	1.74	1.64
Ultimate flexural rigidity E_cI_{expul} (10^9)	kN • mm^2	1.20	1.20	2.69	2.54
Ultimate moment of inertia I_{expul} (10^6)	mm^4	57.14	57.14	128.10	120.95

Fig. 9. Buckling of diagonals of ribs in LT1 and LT4 slab panels.

3.3. Considerations for structural analysis of slab panels

Fig. 12a shows the increment in bending and shear strengths for all specimens with two panels. These increases could be attributed to the distribution of local overloads to the adjacent ribs, as well as the presence of a double truss in the central ribs due to the construction process. According to the observed failure mode (see Figs. 6 and 9), the flexural strength is defined by specimens LT2 and LT3, and shear strength is defined by specimens LT1 and LT4 and shear strength is defined on results from test on specimens LT1 and LT4. Furthermore, Fig. 12a shows that those specimens subjected to 4PBT developed full yielding flexural capacity but could not develop a plastic plateau as the specimens subjected to 3PBT. These specimens also evidenced a faster decrease in flexural stiffness as shown in Fig. 12b. Although all specimens were subjected to the same shear force of 0.50P, the obtained failure modes observed during 3BPT and 4BPT were different due to the bending moment value in each case; for instance, as shown in Table 1, the bending moment value was 1.05P for 3BPT and 0.50P for 4BPT.

Stiffness degradation of the specimen can be measured by a variable called damage index (*DI*) [30] which can be determined according to Eq. (3). This variable can take values between zero and one, where zero represents a non-damaged hinge and one a totally damaged hinge with no stiffness at all, i.e. a totally damaged hinge behaves as internal hinges in elastic frames.

$$DI = \frac{4\left(1 - \frac{K_i}{K_0}\right)}{\left(4 - \frac{K_i}{K_0}\right)} \tag{3}$$

where K_i represents the slope of the elastic unloading during the test as indicated in Fig. 5. The evolution of damage as function of plastic displacement is shown in Fig. 12c. Specimens LT1, LT4, and LT2 present damage values higher than 0.60. Even though there was an overall failure, the damage index (*DI*) does not reach 1; this could be explained by the fact that unlike what occurs in solid elements such as a beam, these panels are formed by two concrete wythes connected by shear connectors; therefore, the concrete wythes in specimens with shear failure mode remain to perform independently, thus the capacity and stiffness correspond to a non-

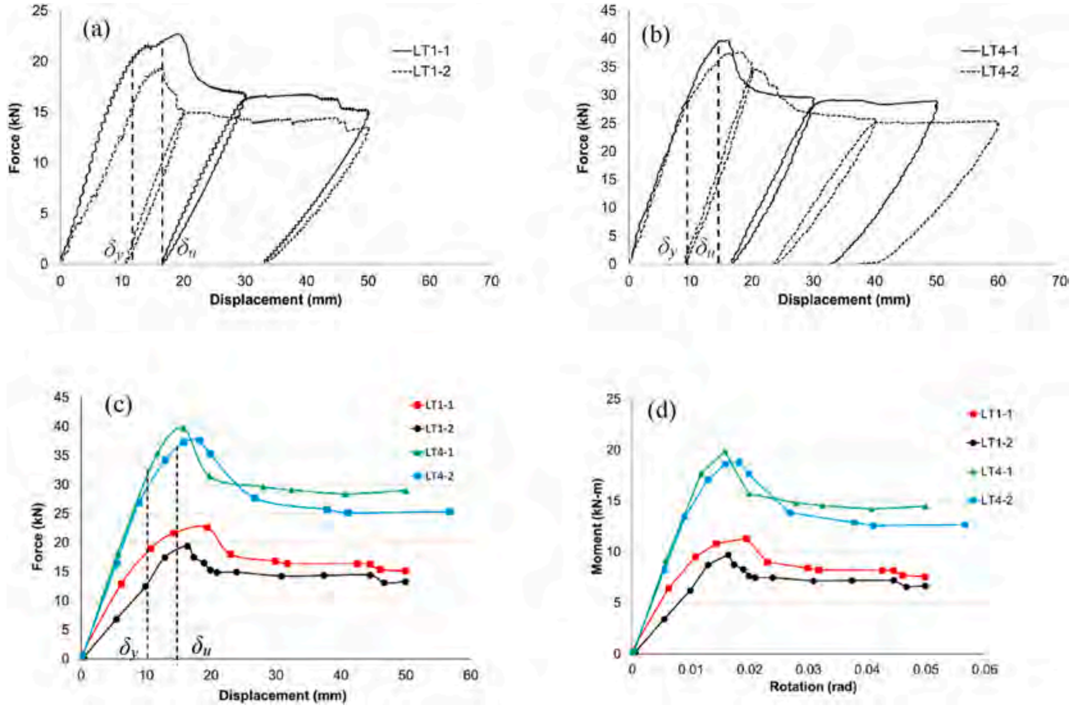

Fig. 10. (a) Force–midspan deflection of specimens LT1, (b) Force–midspan deflection of specimens LT4, (c) Force-midspan deflection envelope, (d) Moment-rotation envelope curve.

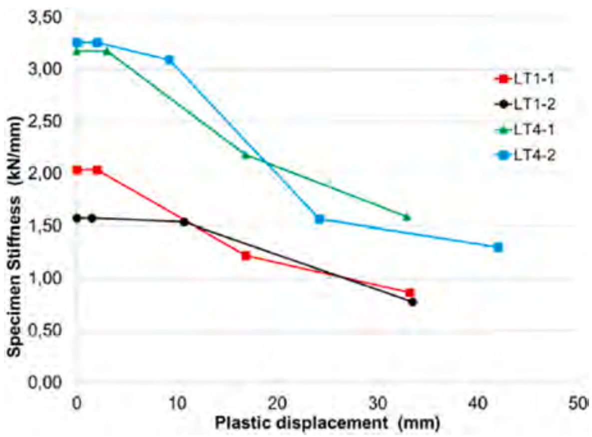

Fig. 11. Elastic slope against plastic displacement 3BPT.

composite element. In specimens with flexural failure mode, the upper concrete wythe remains bearing load acting as a non-composite element. The significant degradation of stiffness, indicating a remarkable damage evolution even with small plastic displacements, could be attributed to the thickness of the wythes and the stiffness of the truss, which can be improved by increasing the diameter of the diagonals and/or decreasing the diagonal spacing.

The mean strength values of each specimen are summarized in Table 4. The mean values of yield and ultimate shear strength of LT1 and LT4 specimens are $V_{ysp} = 7.96$ kN and $V_{usp} = 9.91$ kN, respectively. Similarly, the mean values of yield and ultimate flexural strength of LT2 and LT3 specimens are $M_{ysp} = 7.52$ kN • m and $M_{usp} = 12.34$ kN • m. The mean value of flexural stiffness for a typical 0.60 m-wide slab panel is $E_cI_{sp} = 1.36\text{x}10^9$ kN-mm^2. For the studied panels, the yield force per slab panel that undergo flexural failure was equivalent to that obtained by applying a uniformly distributed load of $w_{ysp} = 5.69$ kN/m^2. The corresponding value for the slabs that undergo shear failure was $w_{ysp} = 8.84$ kN/m^2. This suggests that the main failure mode expected in these slab panels is bending. These values of load are higher than those reported by the codes for residential use and roofs [31]. The distributed loads that resulted in failure by the ultimate flexural moment and ultimate shear force are $w_{usp} = 9.32$ kN/m^2 and 11.01 kN/m^2, respectively.

Table 3
Parameters obtained in 4PBT.

Parameters	Unit	LT1-1	LT1-2	LT4-1	LT4-2
Yield displacement *(δ_y)*	mm	9.2	11.9	10.5	9.4
Span length-deflection ratio $\left(\frac{L_s}{\delta_y}\right)$		326	252	285	318
Ultimate displacement *(δ_u)*	mm	14.2	15.3	15.0	16.4
Ductility factor $\left(\mu = \frac{\delta_u}{\delta_y}\right)$		1.55	1.29	1.43	1.74
Yield load *(P_y)*	kN	17.70	15.52	32.36	28.56
Ultimate load *(P_u)*	kN	21.63	19.12	39.64	37.43
Ultimate-to-yield load ratio *(P_u/P_y)*		1.22	1.23	1.23	1.31
Yield shear force *(V_y)*	kN	8.85	7.76	16.18	14.27
Ultimate shear force *(V_u)*	kN	10.81	9.56	19.82	18.71
Yield bending moment *(M_y)*	kN • m	8.85	7.76	16.18	14.27
Ultimate bending moment *(M_u)*	kN • m	10.81	9.56	19.82	18.71
Elastic Flexural stiffness *(K_0)*	kN/mm	2.03	1.57	3.18	3.26
Experimental flexural rigidity E_cI_{exp} *(10^9)*	kN • mm^2	1.69	1.31	2.65	2.71
Experimental moment of inertia I_{exp} *(10^6)*	mm^4	67.97	51.07	131.87	120.82
Ultimate Flexural stiffness K_{ul}	kN/mm	2.03	1.57	3.18	3.26
Ultimate flexural rigidity E_cI_{expul} *(10^9)*	kN • mm^2	1.69	1.31	2.65	2.71
Ultimate moment of inertia I_{expul} *(10^6)*	mm^4	67.97	51.07	131.87	120.82

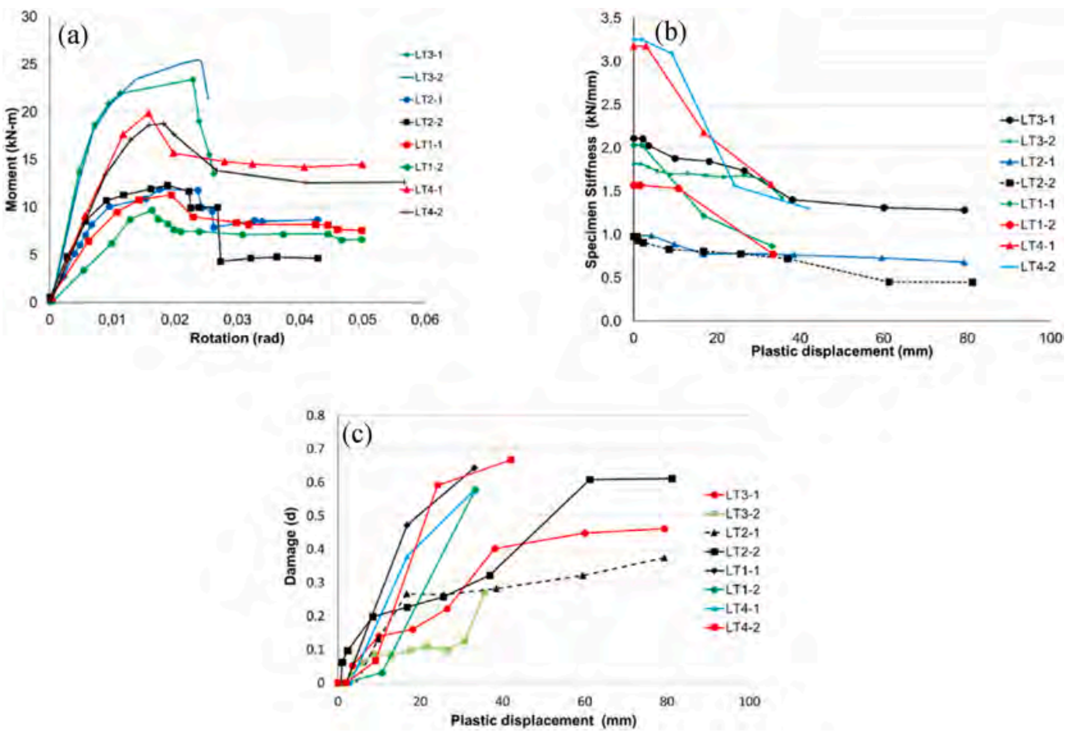

Fig. 12. (a) Moment-rotation curves, (b) Stiffness-plastic displacement curves. (c) evolution of damage index vs plastic midspan deflection.

4. Degree of composite action, DCA

The DCA of each specimen was calculated and analyzed in terms of initial stiffness (K_0) and stiffness at ultimate load (K_{ul}) according to Eqs. (2) and (3). The method used to determine the DCA at the elastic stage (κ) was that proposed by Pessiki and Mlynarczyk [18]. The DCA was calculated by comparing the experimental moment of inertia of the specimens (I_{exp}) with the theoretical moment of inertia of full-composite action (I_c) and non-composite action (I_{nc}). Previous studies [9–11–13] have used three-dimensional finite element models to capture the force/deflection response of sandwich panels and to determine the moment of inertia of full-composite action and non-composite action of slabs. The experimental procedure proposed by Cipollina and Flórez-López [27] is implemented in this study to determine DCA values at ultimate load (κ_u). For the determination of the theoretical moment of the inertia, a simplified cross-section was used as shown in Fig. 13.

Eqs. (4)–(6) were used to calculate the theoretical moment of inertia of non-composite action, I_{nc}, where the wythes are treated as

Table 4
Parameters obtained for the slabs.

Slab panel parameters	Unit	LT2	LT3	LT1	LT4
Yield shear strength (V_{ysp})	kN	3.94	3.22	8.31	7.61
Yield flexural strength (M_{ysp})	$kN \bullet m$	8.28	6.76	8.31	7.61
Ultimate shear strength (V_{usp})	kN	5.88	6.12	10.19	9.63
Ultimate flexural strength (M_{usp})	$kN \bullet m$	12.34	12.33	10.19	9.63
Specimen yield displacement (δ_{ysp})	mm	13.0	9.8	10.6	10.0
Specimen ultimate displacement (δ_u)	mm	41.9	46.2	14.8	15.7
Specimen flexural rigidity E_cI_{mean} (10^9)	$kN \bullet mm^2$	1.42	2.93	1.30	2.51
Slab panel flexural specimen E_cI_{sp} (10^9)	$kN \bullet mm^2$	1.42	1.46	1.30	1.25

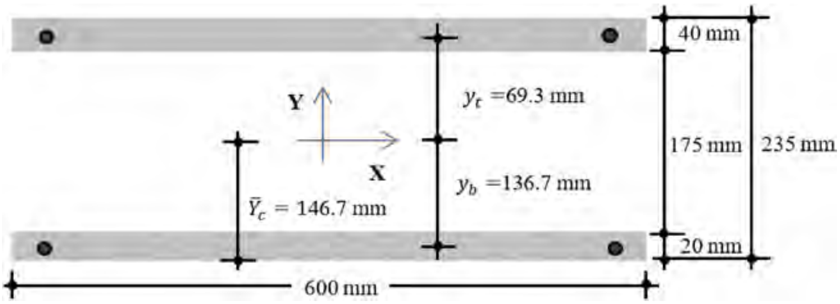

Fig. 13. Transverse section with dimensions.

individual sections.

$$I_t = \frac{bt_t^3}{12} \tag{4}$$

$$I_b = \frac{bt_b^3}{12} \tag{5}$$

$$I_{nc} = I_t + I_b \tag{6}$$

For a fully composite panel, the theoretical moment of inertia I_c depends on the location of the neutral axis of the panel which depends on the thickness of each wythe and was calculated according to Eqs. (7)–(9).

$$A = b(t_t + t_b) \tag{7}$$

$$\underline{Y}_c = \frac{\left[0.50bt_b^2 + bt_t(H - 0.5t_t)\right]}{A} \tag{8}$$

$$I_c = \frac{bt_t^3}{12} + bt_ty_t^2 + \frac{bt_b^3}{12} + bt_by_b^2 \tag{9}$$

Once the experimental moment of inertia of each specimen, $I_{\exp}$ and I_{expul}, is calculated (see Tables 2 and 3), it is used to compare values of κ or κ_{ul} of the specimens according to Eqs. (10) and (11).

$$\kappa = \frac{I_{exp} - I_{nc}}{I_c - I_{nc}}(100) \tag{10}$$

$$\kappa_{ul} = \frac{I_{expul} - I_{nc}}{I_c - I_{nc}}(100) \tag{11a}$$

The values of κ and κ_{ul} of each specimen are summarized in Table 5. The reached values of κ in the specimens ranged between 13% and 22%. The average value of κ was 18.38, and the coefficient of variation (*CV*) was 14.64 %. The average value of κ_{ul} was 16.60, and the correspond *CV* was 10.24 %.

The DCA values and the evolution of the damage index indicate that the stiffness of the truss as a connector is insufficient as a structural element and therefore its characteristics need to be revised. As mentioned earlier, this improvement can be achieved by increasing the diameter of the diagonals and/or decreasing the diagonal spacing.

Table 5
Degree of composite action.

Specimen	Experimental moment of inertia I_{exp} (106 mm^4)	Degree of composite action κ (%)	Ultimate moment of inertia I_{expul} (106 mm^4)	Ultimate degree of composite action κ_{ul} (%)
Composite	339.8	100		
Non-composite	3.6	0		
LT1-1	67.97	18	67.97	18
LT1-2	51.07	13	51.07	13
LT4-1	65.94	18	65.94	18
LT4-2	61.41	16	61.41	16
LT2-1	72.79	21	57.14	16
LT2-2	72.13	20	57.14	16
LT3-1	77.68	22	64.05	18
LT3-2	66.91	19	60.48	17

5. Numerical simulation

In this study, the SAP2000® commercial program was used for the numerical simulation of tested specimens. In order to perform nonlinear static analysis, the slab panels were simulated as nonlinear frame elements using the concept of the lumped plasticity model. All the material properties adopted in the models were those obtained during testing. A two-dimensional model of each panel was established where plastic hinges were assigned to both ends and the midspan of panels. The boundary conditions were assumed hinged at both ends. According to ASCE 41-17 [31], the force-deformation relationships of plastic hinges were represented by five points labeled as A, B, C, D, and E, as shown in Fig. 14. The point "B" is determined using approximate initial effective stiffness of structural elements. In this study, the initial effective stiffness of panels (EI) was modified by κ. According to values obtained in the previous section, the mean flexural stiffness value calibrated for all specimen models was $0.20E_cI_{exp}$.

Two types of plastic hinges were defined; the first one corresponds to flexural failure mode (moment hinge) and the other one corresponds to shear failure mode (shear hinge). Assigned values for each one are summarized in Table 6. Fig. 15 shows the used model for the numerical simulation of a specimen with a single panel.

The load-displacement relationship from the numerical analysis is compared with the experimental results in Fig. 16. The numerical simulation results show a good agreement with that observed in the test. The model predicts the initial stiffness and inelastic behavior until the ultimate load relatively well.

Fig. 17a illustrates the bending moment plastic rotation curves of specimens subjected to 3BPT obtained from numerical simulations. Fig. 17b presents the evolution of plastic rotation with increasing mid-span deflection, while Fig. 17c shows the evolution of the experimental damage index with increasing plastic rotation. Although the evolution of plastic rotation with mid-span deflection appears similar in both specimens, the behavior of the damage index is quite different. This contrast could be attributed to the group action that restrains the progression of damage before failure occurs. Therefore, although an increase in the damage index due to plastic rotation can be inferred, the specific path of the increase must be determined through experimental testing.

Nine concrete sandwich panels reported by Acharya et al. (2022) [17] were selected for validation of the proposed procedure. The tested specimens were classified as short span, medium span, and long span and tested under 4BPT. The displacement was measured at the midspan. Three tests were conducted for each span length. Fig. 18 shows the generalized slab model and typical cross-section of the specimens.

The theoretical moment of inertia of non-composite action $I_{nc} = 3.40\text{x}10^6$ mm^4 and for a fully composite panel is $I_c = 2.59\text{x}10^8$ mm^4. The flexural stiffness of a specimen in the elastic stage (K_0) for each span length is given by Eq. (11).

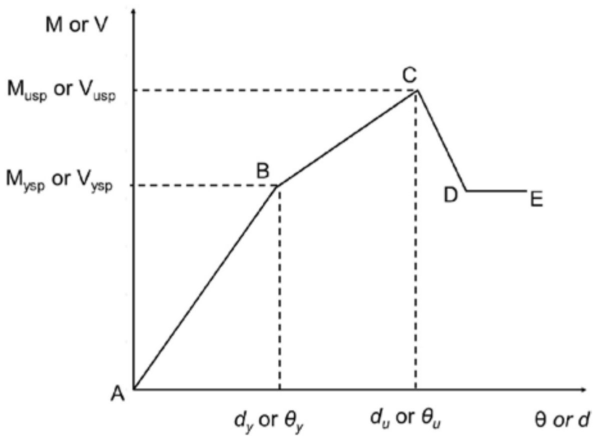

Fig. 14. Generalized force–deformation relationship used for plastic hinges.

Table 6
Assigned values in plastic hinges.

	Moment hinge		Shear hinge	
Point	Moment (kN-m)	Rotation (rad)	Force (kN)	Displacement (m)
A	0.00	0.00	0.00	0.00
B	8.40	0.0006	9.20	0.0100
C	12.40	0.0210	11.60	0.0150
D	8.20	0.0220	8.30	0.0170
E	8.20	0.0260	8.30	0.0200

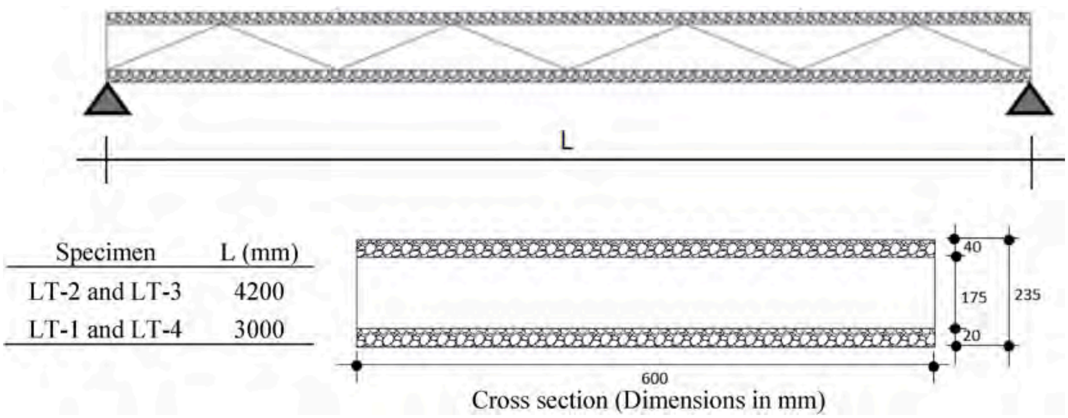

Fig. 15. Numerical model of the slab panel.

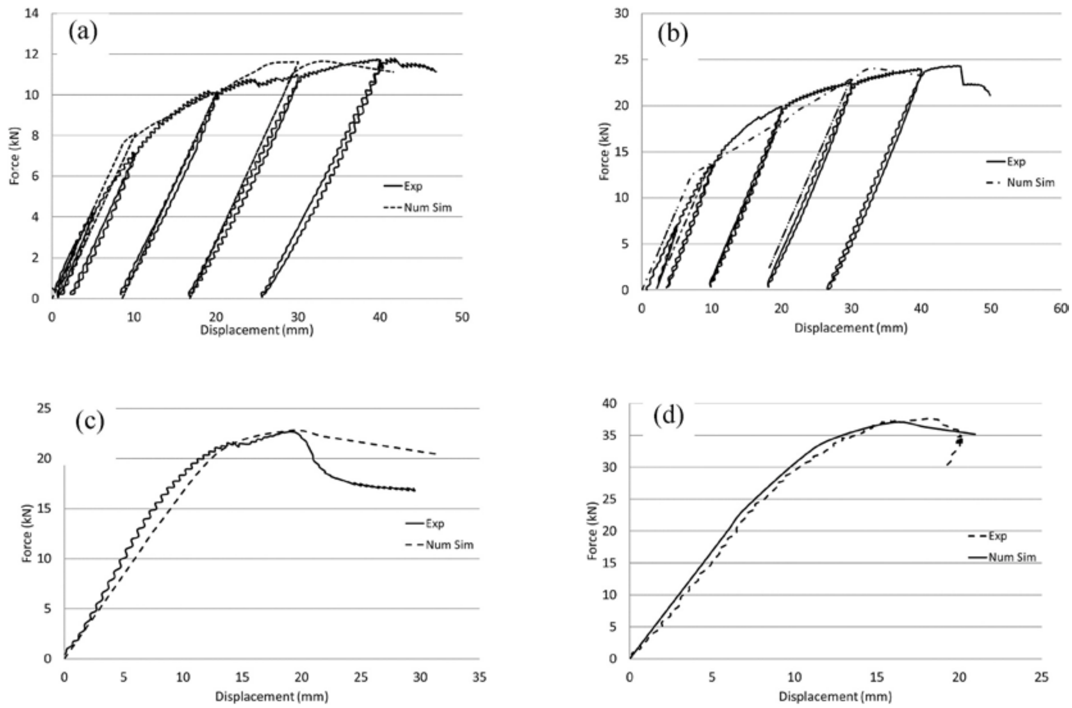

Fig. 16. Numerical simulation compared with experimental results: (a) LT2, (b) LT3, (c) LT1, (d) LT4.

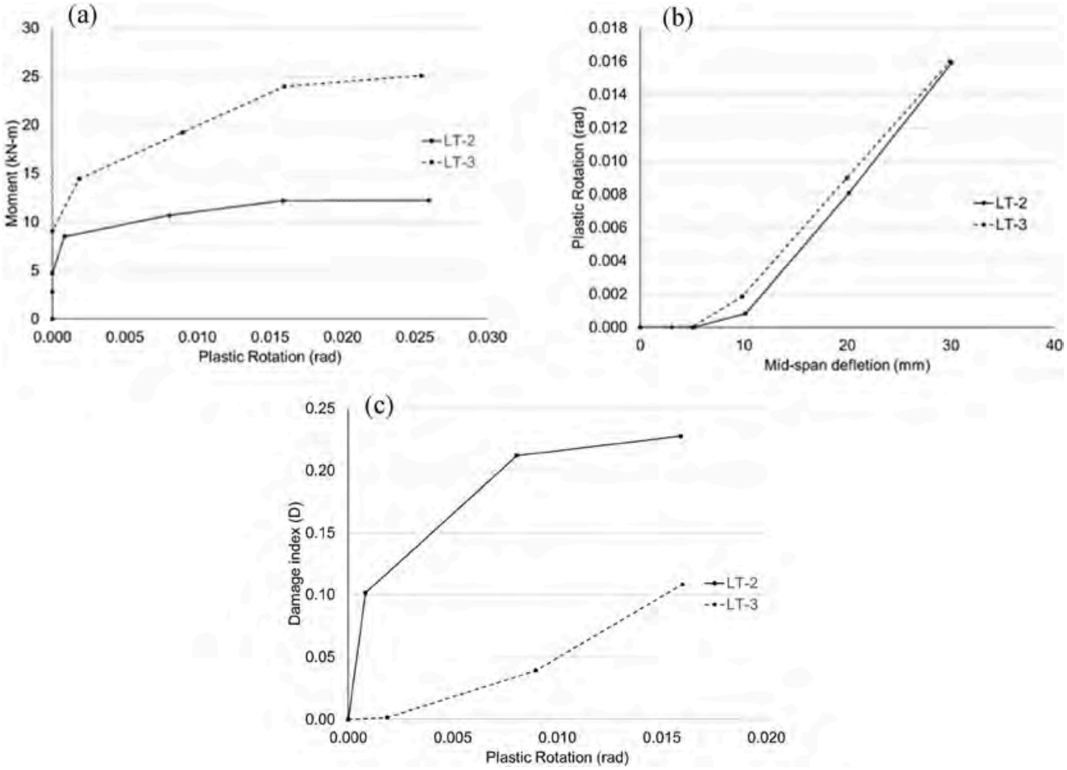

Fig. 17. (a) Bending Moment-Plastic Rotation Curves of Specimens Subjected to 3BPT, (b) Mid-span deflection-plastic rotation curves, (c) Damage index-Plastic rotation.

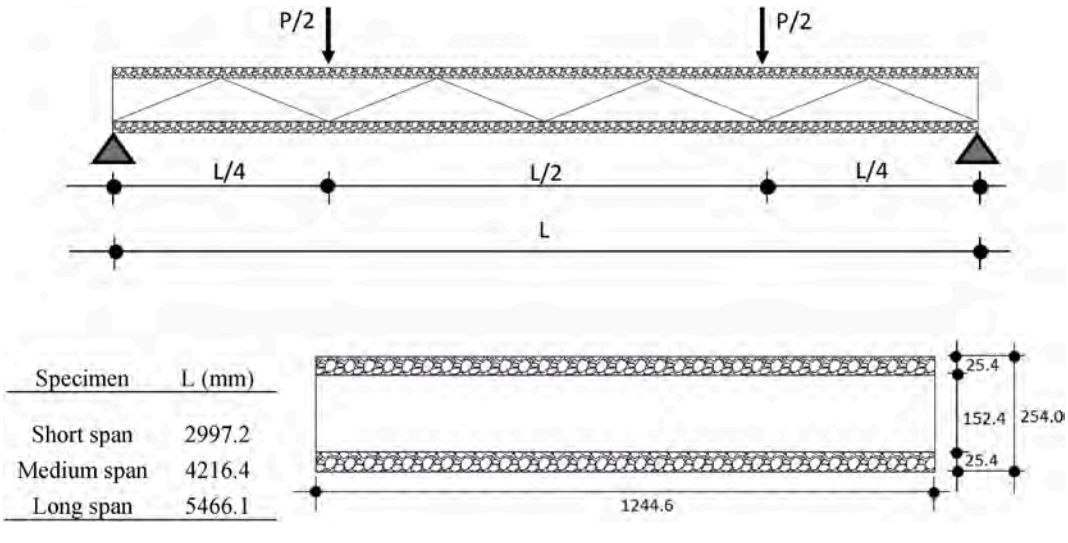

Fig. 18. Slab panel model analyzed by Achary et al. [17].

$$K_0 = \frac{768 E_c I_{exp}}{11 L_s^3} \tag{11b}$$

Table 7 summarizes the obtained experimental test results of the compressive strength of concrete at 28 days (f'_c), modulus of elasticity (E_c), and flexural stiffness in the elastic stage (K_0) of each specimen. These latter results are used to calculate the experimental moment of inertia (I_{exp}) and DCA (κ) according to procedures described in sections 2.2 and 4. Numerical simulations consider the initial effective stiffness of each specimen modified by the average DCA (κ_{ave}). Only one type of plastic hinge was defined and corresponds to flexural failure mode (moment hinge). Assigned values for each specimen are summarized in Table 8.

Table 7
Slab panel parameters.

Specimen		Compressive strength of concrete $f'c$ (MPa)	Modulus of elasticity E_c (GPa)	Elastic Flexural stiffness K_0 (kN/mm)	Experimental moment of inertia I_{exp} (10^7 mm^4)	Degree of composite action κ (%)	Average degree of composite action κ_{ave} (%)
Short-span specimen	A-1	59.69	36.57	12.02	12.65	48	41.3
	A-2	57.54	35.90	12.35	13.23	50	
	A-3	60.21	36.72	6.50	6.81	25	
Medium-span specimen	B-1	51.39	33.93	3.01	9.51	36	30.9
	B-2	49.37	33.25	2.33	7.50	28	
	B-3	52.72	34.37	2.47	7.69	29	
Long-span specimen	C-1	56.43	35.55	1.67	5.03	18	22.7
	C-2	48.94	33.11	2.17	7.02	26	
	C-3	49.01	33.14	1.97	6.38	24	

Table 8
Assigned values in the plastic hinges.

	Specimen A		Specimen B		Specimen C	
Point	Moment (kip-in)	Rotation (rad)	Moment (kip-in)	Rotation (rad)	Moment (kip-in)	Rotation (rad)
A	0	0	0	0	0	0
B	104.12	0.0015	53.54	0.0023	42.22	0.001
C	177.00	0.0141	107.08	0.0092	84.44	0.0075
D	208.24	0.0360	116.72	0.0138	108.51	0.0180
E	144.73	0.0521	85.66	0.0253	67.55	0.0200

The load-displacement relationship from the numerical analysis is compared with the experimental results in Fig. 19. The numerical simulation results show a good agreement with that observed in the test.

Fig. 20 shows the moment curves versus plastic rotation obtained from the numerical simulations. For each scenario, acceptance criteria thresholds can be set based on the expected behavior by established codes. Despite the high ductility values obtained, ranging between 15 and 18, Fig. 21 shows that plastic rotations begin at remarkably low deflection values, above 4 mm. In addition, the evolution of the plastic rotation can be observed with the increase of the mid-span deflection. This correlation could suggest a significant increase in the damage index. However, as mentioned above, this must be determined experimentally due to the characteristics of each panel.

6. Conclusions

This paper proposed a simplified methodology based on a concentrated plasticity model to develop numerical analysis of slab concrete sandwich panels. To validate the proposed methodology, an experimental study was carried out on full-scale slab panels to analyze the flexural behavior. In addition, a proposal for the determination of experimental damage and its evolution within concrete sandwich panels was presented. The results of this study led to the following conclusions:

The proposed methodology proves to be effective and reliable for predicting the behavior of concrete sandwich panels under bending moments. The numerical simulations performed show an adequate description of slab panel behavior until the ultimate load, regardless of its simplicity. This is demonstrated by comparing the model's results with those obtained from the implemented experimental program and other experimental analyses of the literature. This methodology also allows the determination of the usual parameters such as strength capacity, initial stiffness, the flexural damage evolution index, and degree of composite action at ultimate load based on stiffness, for possible structural building analysis.

The significant stiffness degradation, indicating a notable evolution of damage even with small plastic displacements, with the low DCA values, suggests that the studied panels may have limited use as structural elements.

It is recommended to characterize the panels subjected to cyclic loads to determine their performance in areas with seismic or wind hazards. This characterization should include the behavior of both the wall panels and the junction between the slab panel and the wall panel.

In order to be able to analyze the complete behavior of buildings constructed with this system, it is essential to develop a

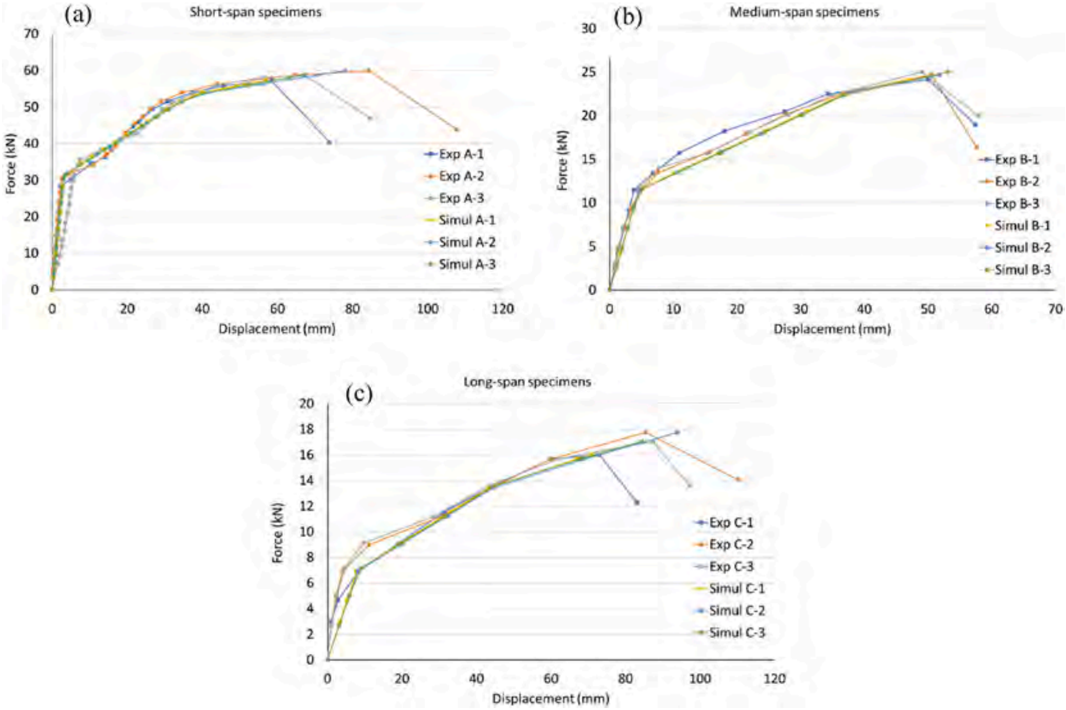

Fig. 19. Numerical simulation compared with experimental results: (a) Short-span specimen, (b) Medium-span specimen, (c) Long-span specimen.

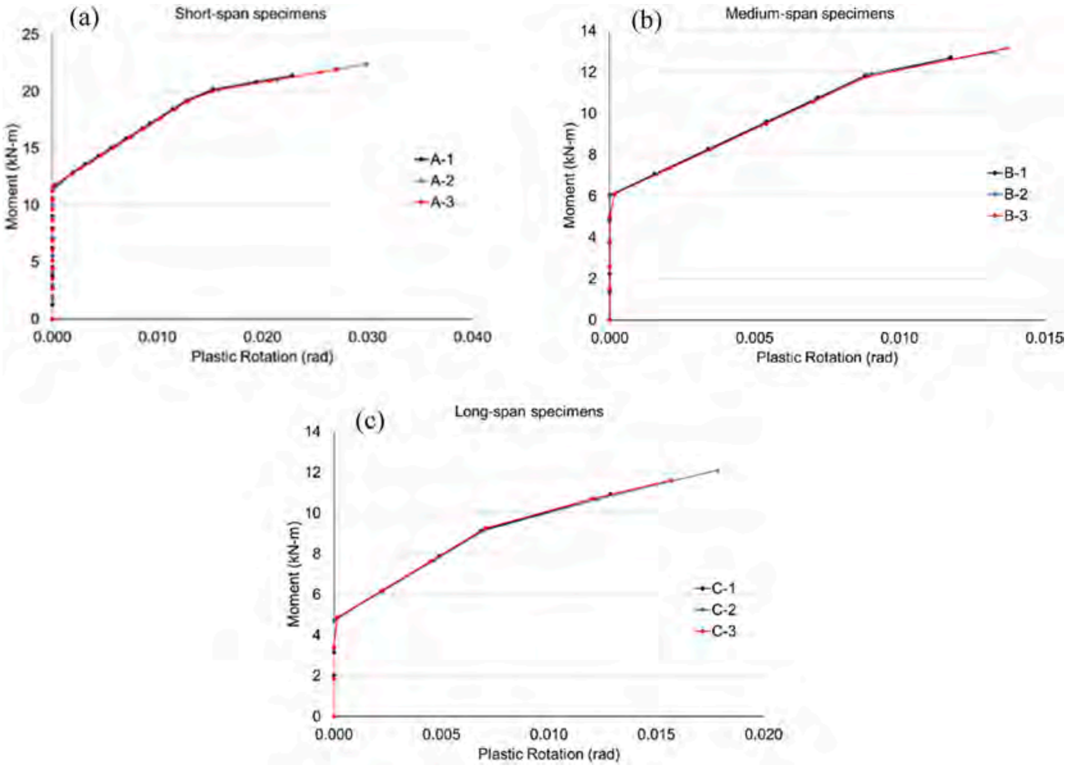

Fig. 20. Moment-plastic rotation curves: (a) Short-span specimen, (b) Medium-span specimen, (c) Long-span specimen.

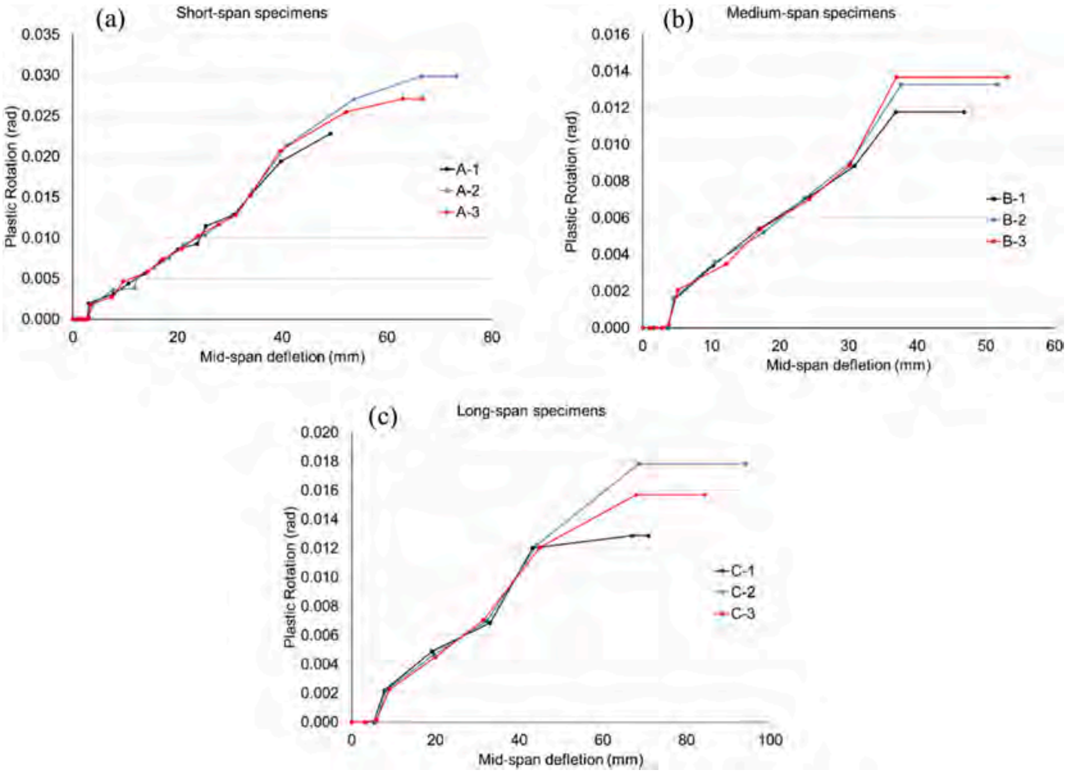

Fig. 21. Mid-span deflection-plastic rotation curves: (a) Short-span specimen, (b) Medium-span specimen, (c) Long-span specimen.

methodology similar to the one presented in this paper, where the simultaneous effects of axial load and bending are included.

CRediT authorship contribution statement

Néstor Guerrero: Writing – review & editing, Writing – original draft, Methodology, Investigation. **Julian Carrillo:** Writing – review & editing, Writing – original draft, Supervision. **Reyes I. Herrera:** Investigation. **MaríaE. Marante:** Writing – review & editing, Supervision, Investigation.

Declaration of competing interest

The authors declare that they have no known competing financial interests or personal relationships that could have appeared to influence the work reported in this paper.

Data availability

No data was used for the research described in the article.

Acknowledgements

The results presented in this paper are part of the research project 'Structural behavior of nontraditional constructions system'. The authors sincerely appreciate the collaboration of the staff of the Laboratory of Structural Mechanics (LME) and the Cerchalosa company for all kinds of support. Julian Carrillo thanks Vicerrectoría de Investigaciones at Universidad Militar Nueva Granada for providing research grants.

References

[1] R. O'Hegarty, O. Kinnane, Review of precast concrete sandwich panels and their innovations, Constr. Build. Mater. 233 (2020) 117145, https://doi.org/10.1016/j.conbuildmat.2019.117145.
[2] A. Einea, D.C. Salmon, G.J. Fogarasi, T.D. Culp, M.K. Tadros, State-of-the-art of precast concrete sandwich panels, PCI J. 36 (6) (1991) 78–92, https://doi.org/10.15554/pcij.11011991.78.98.
[3] A. Benayoune, A.A.A. Samad, D.N. Trikha, A.A.A. Ali, S.H.M. Ellinna, Flexural behaviour of pre-cast concrete sandwich composite panel - experimental and theoretical investigations, Constr. Build. Mater. 22 (4) (2008) 580–592, https://doi.org/10.1016/j.conbuildmat.2006.11.023.
[4] J. Daniel Ronald Joseph, J. Prabakar, P. Alagusundaramoorthy, Experimental study on the flexural behavior of insulated concrete sandwich panels with wires as shear connectors, Alexandria Eng. J. 58 (3) (2019) 901–908, https://doi.org/10.1016/j.aej.2019.08.005.

[5] Y.H. Mugahed Amran, A.A. Abang Ali, R.S.M. Rashid, F. Hejazi, N.A. Safiee, Structural behavior of axially loaded precast foamed concrete sandwich panels, Constr. Build. Mater. 107 (2016) 307–320, https://doi.org/10.1016/j.conbuildmat.2016.01.020.
[6] F. Gara, L. Ragni, D. Roia, L. Dezi, Experimental behaviour and numerical analysis of floor sandwich panels, Eng. Struct. 36 (2012) 258–269, https://doi.org/10.1016/j.engstruct.2011.12.011.
[7] M. del M. Cansario Pérez, A. Aguado, C. i P. de B, Escola Tècnica Superior d'Enginyers de Camins, and Universitat Politècnica de Catalunya., "Sistema constructivo de paneles aligerados con poliestireno expandido y malla electrosoldada espacial estudio estructural y optimización,", Universitat Politècnica de Catalunya., Spain, 2005. http://hdl.handle.net/2117/93477.
[8] I. Choi, J.H. Kim, H.R. Kim, Composite behavior of insulated concrete sandwich wall panels subjected to wind pressure and suction, Materials 8 (3) (2015) 1264–1282, https://doi.org/10.3390/ma8031264.
[9] M. Flansbjer, N. Williams Portal, D. Vennetti, U. Mueller, Composite behaviour of textile reinforced reactive Powder concrete sandwich façade elements, Int. J. Concr. Struct. Mater. 12 (1) (2018), https://doi.org/10.1186/s40069-018-0301-4.
[10] N. Williams Portal, M. Flansbjer, K. Zandi, L. Wlasak, K. Malaga, Bending behaviour of novel Textile Reinforced Concrete-foamed concrete (TRC-FC) sandwich elements, Compos. Struct. 177 (2017) 104–118, https://doi.org/10.1016/j.compstruct.2017.06.051.
[11] M. Mastali, I.B. Valente, J.A.O. Barros, Development of innovative hybrid sandwich panel slabs: advanced numerical simulations and parametric studies, Compos. Struct. 152 (2016) 362–381, https://doi.org/10.1016/j.compstruct.2016.05.072.
[12] M. Mastali, I.B. Valente, J.A.O. Barros, Flexural performance of innovative hybrid sandwich panels with special focus on the shear connection behavior, Compos. Struct. 160 (2017) 100–117, https://doi.org/10.1016/j.compstruct.2016.10.066.
[13] A. Chen, T.G. Norris, P.M. Hopkins, M. Yossef, Experimental investigation and finite element analysis of flexural behavior of insulated concrete sandwich panels with FRP plate shear connectors, Eng. Struct. 98 (2015) 95–108, https://doi.org/10.1016/j.engstruct.2015.04.022.
[14] A. Shams, M. Horstmann, J. Hegger, Experimental investigations on textile-reinforced concrete (TRC) sandwich sections, Compos. Struct. 118 (1) (2014) 643–653, https://doi.org/10.1016/j.compstruct.2014.07.056.
[15] R. O'Hegarty, R. West, A. Reilly, O. Kinnane, Composite behaviour of fibre-reinforced concrete sandwich panels with FRP shear connectors, Eng. Struct. 198 (2019), https://doi.org/10.1016/j.engstruct.2019.109475.
[16] I.G. Colombo, M. Colombo, M. Di Prisco, Bending behaviour of textile reinforced concrete sandwich beams, Constr. Build. Mater. 95 (2015) 675–685, https://doi.org/10.1016/j.conbuildmat.2015.07.169.
[17] M. Acharya, K. Gurung, M. Mashal, Full-scale flexural testing of slabs made of modular structural concrete insulated panels, PCI J. 67 (2) (2022) 55–76, https://doi.org/10.15554/pcij67.2-03.
[18] S. Pessiki, A. Mlynarczyk, Experimental Evaluation of the precast concrete walls, PCI J. March-Apri (2) (2003) 54–73 [Online]. Available: http://www.pci.org/uploadedFiles/Siteroot/Publications/PCI_Journal/2003/DOI_Articles/jl-03-march-april-5.pdf.
[19] T. Zheng, Q. Ge, F. Xiong, G. Li, Y. Xue, X. Deng, Study of the flexural performance and a novel calculation formula for the degree of composite action for precast concrete sandwich panels, Struct. Des. Tall Spec. Build. (April) (2023) 1–16, https://doi.org/10.1002/tal.2065.
[20] D. Tomlinson, A. Fam, Analytical approach to flexural response of partially composite insulated concrete sandwich walls used for cladding, Eng. Struct. 122 (2016) 251–266, https://doi.org/10.1016/j.engstruct.2016.04.059.
[21] I.G. Colombo, M. Colombo, M. di Prisco, F. Pouyaei, Analytical and numerical prediction of the bending behaviour of textile reinforced concrete sandwich beams, J. Build. Eng. 17 (August 2017) (2018) 183–195, https://doi.org/10.1016/j.jobe.2018.02.012.
[22] T.P.A. Dunn, G.P.A.G. van Zijl, A.S. van Rooyen, Investigating a reinforced lightweight foamed concrete walling system for low-rise residential buildings in moderate seismic regions, J. Build. Eng. 20 (September) (2018) 663–670, https://doi.org/10.1016/j.jobe.2018.09.011.
[23] G. Xu, T. Guo, A. Li, Seismic performance and fragility analysis of precast concrete sandwich wall structure, J. Earthq. Eng. 00 (00) (2021) 1–24, https://doi.org/10.1080/13632469.2021.2003272.
[24] G. Xu, A. Li, Seismic performance of a new type precast concrete sandwich wall based on experimental and numerical investigation, Soil Dyn. Earthq. Eng. 122 (November 2018) (2019) 116–131, https://doi.org/10.1016/j.soildyn.2019.04.013.
[25] F. Gara, L. Ragni, D. Roia, L. Dezi, Experimental tests and numerical modelling of wall sandwich panels, Eng. Struct. 37 (2012) 193–204, https://doi.org/10.1016/j.engstruct.2011.12.027.
[26] M.J. Gombeda, P. Trasborg, C.J. Naito, S.E. Quiel, Simplified model for partially-composite precast concrete insulated wall panels subjected to lateral loading, Eng. Struct. 138 (2017) 367–380, https://doi.org/10.1016/j.engstruct.2017.01.065.
[27] A.J.F.-L. Cipollina, Modelos simplificados de daño en porticos de concreto armado, Rev. Int. Métodos Numéricos Cálculo Diseño Ing. 11 (1993) 1–20.
[28] F. Bai, J.S. Davidson, Analysis of partially composite foam insulated concrete sandwich structures, Eng. Struct. 91 (2015) 197–209, https://doi.org/10.1016/j.engstruct.2015.02.033.
[29] ACI318-19, *318M-19: Building Code Requirements For Concrete and Commentary*, American Concrete Institute, Famington Hills, MI, 2019, https://doi.org/10.14359/51716937.
[30] A. Cipollina, A. López-Inojosa, J. Flórez-López, A simplified damage mechanics approach to nonlinear analysis of frames, Comput. Struct. 54 (6) (1995) 1113–1126, https://doi.org/10.1016/0045-7949(94)00394-I.
[31] ASCE/SEI 41–17, *Seismic Evaluation And Retrofit Of Existing Buildings*, American Society of Civil Engineers, Reston, VA, 2017, https://doi.org/10.1061/9780784414859.